River Flow 2010 - Dittrich, Koll, Aberle & Geisenhainer (eds) - © 2010 Bundesanstalt für Wasserbau ISBN 978-3-939230-00-7

Flow around submerged groynes in a sharp bend using a 3D LES model

S. Kashyap, C. D. Rennie & R. Townsend
Department of Civil Engineering, University of Ottawa, Canada

G. Constantinescu, T. E. Tokyay
Civil and Environmental Engineering Department & IIHR-Hydroscience and Engineering, The University of Iowa, Iowa City, Iowa, USA

ABSTRACT: Large Eddy Simulation (LES) is used to elucidate the main features of the 3D turbulent flow field around submerged groynes in a sharp channel bend with a flat bed at a channel Reynolds number close to 60,000. Submerged groynes are underwater structures that direct flow away from river banks in order to reduce erosion. In the present study the groynes are submerged at a submergence ratio (channel depth/groyne height) of 1.8, which is characteristic for groynes at high flood conditions, and the conditions when the greatest scour occurs. LES is used to understand the main circulatory motions within the embayments and at the interfaces between the groyne field and the main channel. LES shows that flow at the inner bank of a strongly curved bend is characterized by strong streamwise oriented vortices that can locally erode the bed and channel sidewalls. LES successfully captures the unsteady dynamics of horseshoe vortices forming at the groyne tips. For the present groyne layout, horseshoe vortices increase bed shear and pressure fluctuations, and are likely the main mechanism inducing channel scour. Finally, the predicted distribution of bed friction velocity identifies regions where sediment entrainment would occur at conditions corresponding to the start of scour.

Keywords: Submerged groynes, Spur dikes, Large eddy simulation, River bank erosion, Bends

1 INTRODUCTION

Groynes are flow diversion structures, commonly used in river engineering to prevent bank erosion and control river meandering. They may serve additional functions such as improving channel navigability by deepening the river centerline, and improving aquatic habitats by creating low velocity scour pools around their toes where fish can rest and feed. Groynes have typically a trapezoidal section with a gentle surface slope, and they project out from the bank at an angle (USDA 2005). For the purpose of bank protection, it is best for them to be pointed in the upstream direction. Commonly they are also referred to in the literature as spur dykes, rock vanes, weirs and stream barbs. Normally constructed from rock, they may be submerged or emergent with respect to normal water levels. A better understanding of the flow dynamics around groynes is important, particularly under submerged conditions when they are more likely to cause bank erosion (Yossef 2005; US Department of Transportation 1985). More knowledge is needed on how groynes perform in river bends of high curvature where they have shown considerable scour in the field (WST Inc. 2002). This paper investigates some of the main flow features around submerged groynes in a sharp river bend using a highly resolved 3D Large Eddy Simulation (LES). The present LES model has already been used to study the flow and mass exchange processes past emerged and submerged groynes situated in straight channels (e.g., see McCoy et al., 2007, 2008 and Constantinescu et al., 2009). Studies of similar submerged structures in a straight channel (Kuhnle et al. 2008) and in a meander bend (Abad et al. 2008) have been conducted using Reynolds Averaged Navier Stokes (RANS) models. In the present work, LES is used for the first time to study the physics of flow past submerged groynes in a sharp bend.

2 NUMERICAL SOLVER

The Large Eddy Simulation (LES) code used in the present work (Mahesh et al. 2004) employs a finite volume method to solve the 3D spatially fil-

tered Navier Stokes equation, given by Equation (1) in tensor notation, on a hybrid unstructured grid.

$$\frac{\partial \bar{u}_i}{\partial t} + \frac{\partial \overline{u_i u_j}}{\partial x_j} = -\frac{\partial \bar{p}}{\partial x_i} + \nu \frac{\partial^2 \bar{u}_i}{\partial x_j x_j} + \frac{\partial \tau_{ij}}{\partial x_i} \quad (1)$$

Here spatial filtering is denoted by the overbar (-), ν is the kinematic viscosity and τ_{ij} is the subgrid (SGS) stress. The LES code is a parallel (MPI) solver that uses a collocated finite-volume scheme to solve the filtered Navier-Stokes equations with the Smagorinsky model (Mahesh et al. 2004). In the predictor-corrector formulation the Cartesian velocity components defined at the center of the cell and the face-normal velocities defined at the center of the face are essentially treated as independent variables. The fractional step algorithm is second order accurate in both space and time. All the operators in the code, including the convective terms, are discretized using central schemes. The numerical scheme used to solve the Navier-Stokes equations discretely conserves energy. This increases the robustness of the numerical algorithm without the use of numerical dissipation which is essential for accurate LES. Time discretization is achieved using a Crank Nicholson scheme for the convective and viscous operators in the momentum (predictor step) equations. The system resulting due to the implicit time discretization is solved using the Successive over-relaxation (SOR) method. The pressure equation is solved using a conjugate gradient method with preconditioning. No wall functions are used and the governing equations are integrated through the viscous sub-layer.

3 SIMULATION SETUP

The numerical simulation was modeled after a physical groyne experiment set up at the University of Ottawa. The experiment considered cases with a flat fixed bed and an erodible bed, with and without groynes. The numerical model described in the present paper simulated flow in a sharp 135º bend with three groynes over a flat fixed bed, assuming hydraulically smooth conditions. The flow in the experiment was also very close to being hydraulically smooth. The main flow parameters are given in Table 1 and the computational domain is shown in Figure 1. The mean water depth (H) in the experiment was 0.15 m, and was used as the length scale for nondimensionalizing the flow and geometrical variables in the simulation. The mean velocity (u) in the incoming flow was used as the velocity scale. The modeled flume contained a straight inlet section of length L=14.55H, a sharp 135° bend with a radius of curvature (centerline radius/channel width) of 1.5, and a straight exit section of length L=11.89H. The dimensions of the groynes are shown in Figure 2. The size, spacing and location of the groynes were based on previous studies conducted at the University of Ottawa (Matsurra 2004; Minor et al. 2007), and design guidelines from the USDA (2005). The groyne top crest sloped downwards from the bank at an angle of 6.5° with the horizontal, and the groyne side walls were vertical. The submergence ratio (H/d), where d is the groyne height, ranged from 1.85 at the (bank-wise) base of the groyne to 4.29 at the (stream-wise) toe. The width ranged from 0.57H at the base to 0.33H at the toe, and the groyne centerline length was 4.00H. The groyne centerline made an (upstream-side) angle of 25° with the tangent to the outer bank. The first upstream groyne base was placed at the point where erosion first impacted the outer wall, as determined from an experimental calibration run. Placements of subsequent downstream groynes were determined using the midpoint spacing method recommended by the USDA (2005) and used by Matsurra (2004), with the spacing along the outer wall between the groyne centerlines being 4.77H.

Table 1. Flow parameters for the model where u is the main channel average velocity, H is the water depth, u_* is the bed friction velocity, u_{*cr} is Shields' critical friction velocity, $d50$ is the sediment mean diameter, Re_* is the Reynolds number defined with the bed friction velocity, and Fr is the channel Froude number.

u (m/s)	H (m)	u^* (m/s)	u^*_{cr} (m/s)
0.310	0.150	0.0152	0.0197
$d50$ (mm)	Re^*	Re (uH/ν)	Fr
0.689	13.8	61,300	0.255

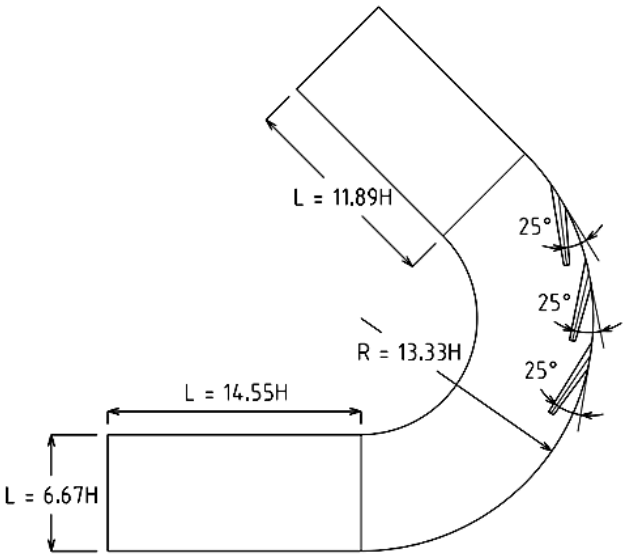

Figure 1. Plan view of flume showing main dimensions and groyne layout.

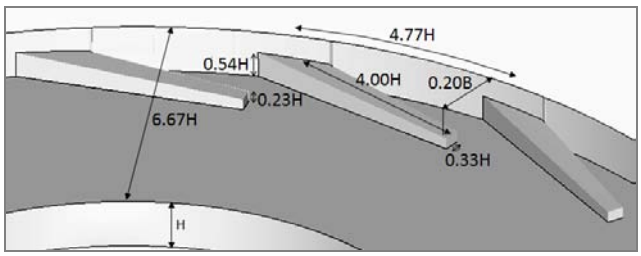

Figure 2. Three dimensional view of the channel in the region where the groynes are present.

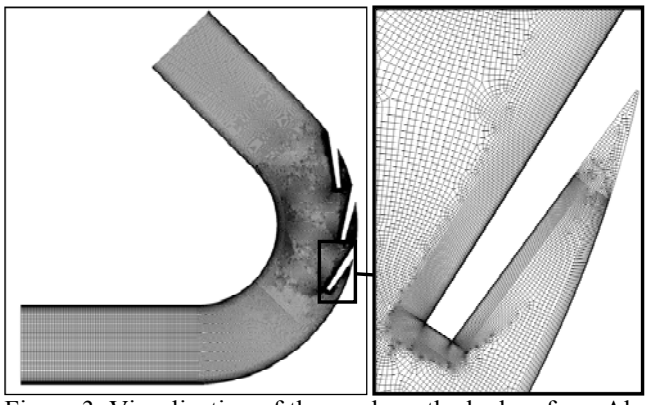
Figure 3. Visualization of the mesh on the bed surface. Also shown is a detailed view of the mesh around the first groyne.

The mean inflow velocity profile was obtained from a preliminary RANS simulation conducted at the same Reynolds number. Zero mean turbulent velocity fluctuations obtained from a preliminary LES simulation in a periodic channel were added on top of the mean velocity profiles. The constant flow discharge was $6.67UH^2$. The free surface was modeled as a symmetry boundary condition, assuming a rigid lid approximation. This is acceptable (see discussion in Zeng et al., 2008) due to the low (<0.3) Froude number (Table 1). A convective outflow boundary condition was used at the outlet. All solid boundaries of the channel and groynes were treated as no slip smooth surfaces.

The unstructured mesh contained only hexahedral cells and was generated using a paving technique in horizontal planes (Figure 3). It consisted of a total of 6.6 million grid points including 50 grid points in the vertical direction. The grid cell closest to the bed and lateral walls had a non dimensional size of $(\Delta n/H)$~0.0009 or less than three wall units. The maximum cell at the surface had $\Delta n/H$~0.0907 or about 300 wall units.

4 DISCUSSION

All results presented in this paper, other than Figure 6, describe the mean flow field and turbulence structures predicted by the LES. The results from the simulation with groynes showed velocity patterns away from the groyne region that were qualitatively similar to other studies of flow in sharp bends (centerline radius/channel width <3) with no groynes and a flat bed. As with the RANS study by Zeng et al. (2008), which was conducted at initial flat bed conditions, but without groynes, the core of high streamwise velocity is gradually advected by secondary circulation from the inner to the outer bend (Figure 4a). There is strong vertical non-uniformity in the advection of the core towards the outer bank. Surface velocities at Z/H = 0.95 (Figure 4a) are being advected more quickly than near-bed velocities at Z/H = 0.25. While a region of low streamwise velocity develops away from the bed close to the inner wall starting at 25º in the bend region (Figure 4a, Z/H = 0.5, 0.95), the core of high streamwise velocity near the bed remains close to the inner bank in the groyne region (Figure 4a, Z/H = 0.25). This is expected as the groynes extend to less than half the channel depth. Thus, a relatively large amount of the high speed incoming flow can be convected between the top of the embayments and the free surface. However, past the groyne region, the position of the core of high streamwise velocity is relatively similar at all levels. One suspects that for emerged groynes, the position of the region of high streamwise velocity will be similar to that predicted at Z/H = 0.25 (Figure 4a) at all flow depths, and flow non-uniformity in the vertical direction would have been much lower.

As discussed previously, the effect of the groynes is to reduce the strong streamwise velocity gradients that would otherwise develop at the outer bank of a strongly curved bend. One should point out that in the case of submerged groynes, high velocities may still occur at the outer bank above the top of the groynes, particularly near the junction between the groynes and outer bank. Depending also on the orientation, spacing, and geometry of the groynes, large streamwise velocities may induce bank erosion especially for a highly inclined outer bank.

The ability of the groynes in counteracting the main cell of secondary circulation induced by the bend is seen in Figure 4b. For the present flow conditions and geometry, the main cell of recirculation region cannot penetrate out to the outer wall in the groyne field region (e.g. 90^0 section). As a result, the core of high streamwise velocity does not penetrate the lateral interface of the embayments. As this is the case not only over the embayment depth, but over the whole channel depth, one can conclude that the groynes effectively protect the outer bank region for submergence depths that are less or equal than the one used here.

The secondary flow pattern inside and over the embayments is complex. Streamlines at 90^0 suggest the presence of a secondary counter-rotating

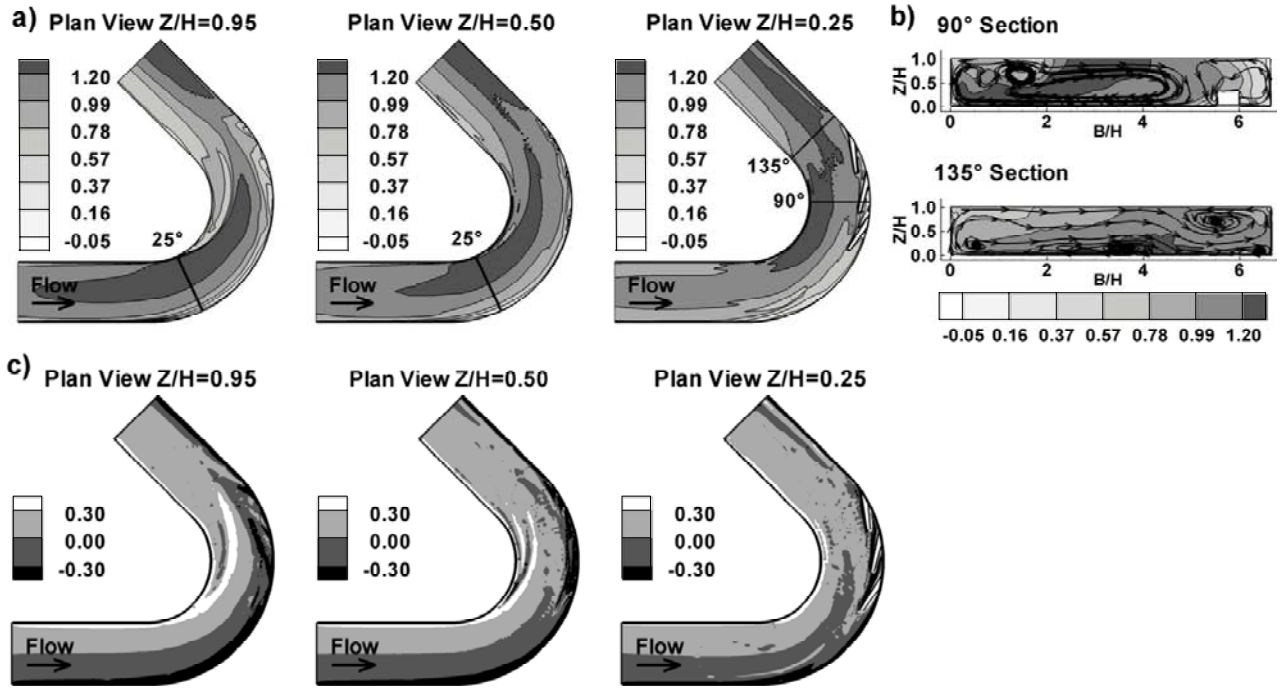

Figure 4. 2D Distribution of the nondimensional mean streamwise velocity (+=in flow direction,-=opposite flow direction) in a) horizontal planes situated at *Z/H*=0.95, 0.50 and 0.25, and b) in the 90º and 135º cross sections. Frame (c) shows the distribution of the nondimensional mean vertical vorticity component (+=upwards/counter-clockwise,-=downwards/clockwise) in horizontal planes situated at *Z/H*=0.95, 0.50 and 0.25.

weak cell of recirculating flow. However, the important point is that streamwise velocity gradients within the embayment are small, both close to the outer bank and channel bed. As the largest contribution to friction velocity is due to these velocity gradients, one expects erosion to be greatly reduced compared to when groynes are not present.

Downstream of the groyne region (e.g. 135^0 section), another cell of secondary circulation with a rotation direction opposite to that of the main recirculation cell is present. This counter rotating cell prevents the core of high streamwise velocity from reaching the top part of the outer bank, at least for a certain distance (~3*H*) downstream of the last groyne. This cell acts similarly to the classical secondary recirculation cells forming at the outer bank of curved bends. However, its formation, strength and extent are determined to a large extent by the presence of the groynes.

Next, we focus on the flow structure close to the inner bend. The information given by Figures 4a and 4c is directly related, in the sense that the position of regions of high streamwise velocity gradients in Figure 4a is correlated to the position of regions of high streamwise vorticity in Figure 4c (one borders the other). The most obvious feature in the vorticity field at $Z/H = 0.95$ is the presence of a strong shear layer at the inner bank. This shear layer originates close to 25º into the bend region. At mid-depth level, a second shear layer is observed in between the inner bank and the first shear layer. These shear layers disappear in the lower part of the channel. One should emphasize that, in horizontal planes, the flow is oriented in the streamwise direction at all spanwise locations between the inner bank and the center of the section. Thus, the shear layers do not correspond to the boundary between a separated eddy and the main channel flow. Rather, they are induced by the strong non-uniformity of the streamwise velocity profile in the spanwise direction over the upper part of the channel. The presence of these regions of strong streamwise shear in a region of high channel curvature induces the formation of several streamwise-oriented vortices. The locations of these vortices are depicted in Figures 5a and 5b using the Q criterion, and in Figure 5c using streamlines.

At first, one might link the formation of the two shear layers and the associated secondary streamwise oriented vortices only to the presence of the submerged groynes that obstruct the flow over the lower part of the channel inside the bend region. However, the EPFL experiment of the flow in a strongly curved bend without groynes (Zeng et al., 2008) has shown the formation of a similar secondary flow pattern close to the inner bend. Thus, the high vertical non-uniformity of the flow close to the inner bank, and the associated formation of streamwise oriented vortices and shear layers, is a general characteristic of sharp bend flows. We plan to investigate further the influence of the groynes on the strength of the streamwise oriented vortices at the inner bank by comparing results of the present LES simulation with a simulation performed in the same channel

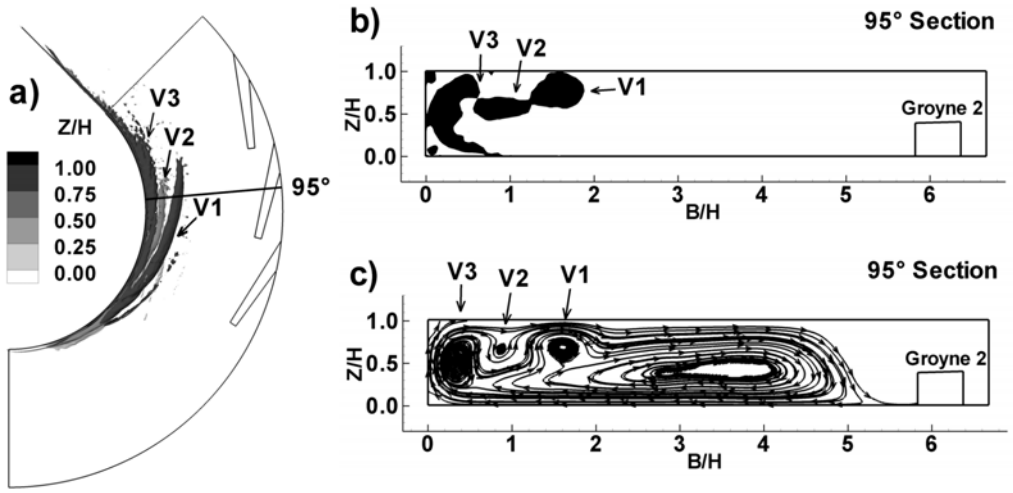

Figure 5. Visualization of the vortical structure of the mean flow close to the inner bank using a) Q criterion – 3D view from above, b) Q criterion in the 95° cross section, c) 2D streamlines in the 95° cross section. V1 and V3 are rotating clockwise, and V2 is rotating counter-clockwise.

but without groynes. To capture accurately the position, extent and location of these shear layers, and associated vortices, the use of LES is essential. This is because these streamwise oriented vortices forming in bends of high curvature are driven largely by curvature-induced anisotropic effects.

Figure 5 shows three streamwise oriented vortices (V1, V2, and V3) near the inner bank. At approximately 35º, the clockwise rotating vortex V1 forms close to the inner bank. As one moves downstream, V1 grows in size and then starts decaying past 90^0. At about 65º, V1 gets away from the inner bank. Concurrently, a second clockwise rotating vortex, V3, forms close to the inner bank. The two vortices are separated by a weaker counter clockwise rotating vortex, V2, situated at a slightly lower elevation (Figure 5b). As inferred from Figure 4c, V1 is situated in the region of low streamwise velocities forming on the left side (toward the inner bank) of the central core of high streamwise velocity. In fact, up to 65^0 V1 is situated in between the inner bank and the first shear layer. Past 65^0, V1 is situated in between the two separated shear layers. In the 90^0 section, V3 convects higher streamwise velocity fluid towards the inner bank. Thus, the presence of V3 increases the streamwise component of the friction velocity on the inner bank wall, as well as the spanwise component of the bed friction velocity on the inner bank side of the shear layer. The role of V1, before it gets away from the inner bank (past 65^0 section), is similar. Thus, these streamwise oriented vortices may induce additional erosion close to the inner bank during initial stages of scour. In this regard, their role is opposite to that of the secondary cell forming at the outer bank of a curved channel.

The Q criterion is used to visualize in Figure 6 the necklace vortices present in the instantaneous flow around the tip of groyne 2. The stronger primary necklace vortex is situated next to the tip of the groyne. Upstream of it, a secondary necklace vortex is present. The legs of these vortices in the main channel side of the groyne are deflected away from the groyne sidewall, and into the main channel flow. Both vortices are also present in the mean flow where they are visualized using vorticity magnitude contours in Figure 7b and 2D streamline patterns in Figure 7c.

Several hairpin-like eddies induced by a secondary instability developing along the core of the primary vortex wrap around it. Similar to the numerical study of the horseshoe vortex system forming at a base of a rectangular cylinder conducted by Kirkil and Constantinescu (2009), these eddies are not present when the Q criterion is used to visualize the structure of the horseshoe vortex system in the mean flow. A small junction vortex is also present at the base of the tip of the groyne.

The distribution of turbulent kinetic energy (TKE) in the vertical plane cutting through the centerline of groyne 2 is shown in Figure 7a. A large elliptical patch of high TKE is observed around the location of the core of the main necklace vortex. The TKE distribution within this patch shows the presence of two peaks.

The large amplification of the TKE inside the region where the core of the main necklace vortex oscillates, and the two-peak distribution of the TKE are induced by low-frequency bimodal oscillations of its core in the vicinity of the tip of the groyne (e.g., see Devenport and Simpson, 1990, Koken and Constantinescu, 2008, 2009 and Kirkil and Constantinescu, 2009 for a detailed description of the characteristics of the turbulence within

the horseshoe vortex system forming in front of a bluff body and of the flow structure in the two dominant modes). Additionally, a second small patch of high TKE values is present in the near bed region where the downstream part of the jet-like flow developing beneath the core of the primary necklace vortex changes direction, as the vortex switches between the zero-flow mode (the core is close to circular and is situated closer to the obstacle) and the back-flow mode (the core is more elliptical and is situated far from the face of the obstacle). This second patch of high TKE values was also observed in eddy-resolving simulations of the flow past circular and rectangular cylinders and past an isolated groyne in a straight channel at $10^5<Re<10^6$ (Kirkil and Constantinescu 2009; Koken and Constantinescu 2009), and in the measurements of Devenport and Simpson (1990) for flow past a wing-shaped body at Re~125,000.

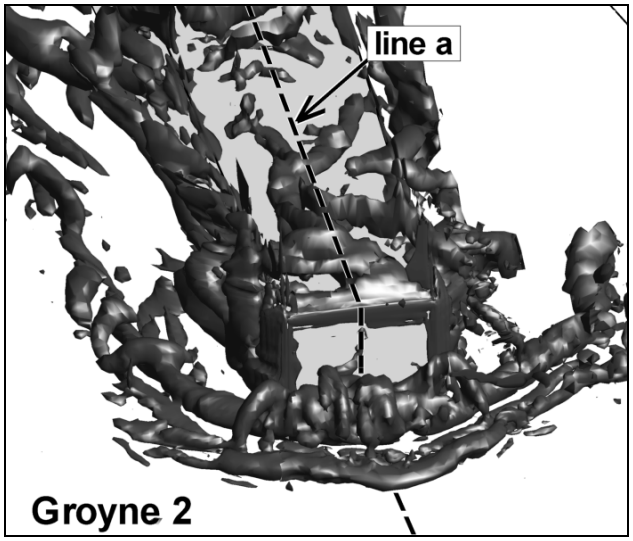

Figure 6. Visualization of the horseshoe vortex system around groyne 2 in the instantaneous flow. Line a shows the location of the vertical section cutting along the centerline of groyne 2. The structure of the horseshoe vortex system in the mean flow is analyzed in Figure 7.

In contrast to the high levels of TKE within the region where the core of the primary necklace vortex is subject to large-scale aperiodic oscillations, levels of TKE remain low in the region of the secondary necklace vortex core (Figure 7a). This happens despite the fact that coherence of the secondary necklace vortex is relatively high, and its circulation is non-negligible compared to that of the primary vortex (Figure 7b). Koken and Constantinescu (2008) have shown this is because the core of the secondary necklace vortice is not subject to bimodal oscillations which are the main reason for the strong TKE amplification (by about one order of magnitude compared to the TKE in the incoming flow).

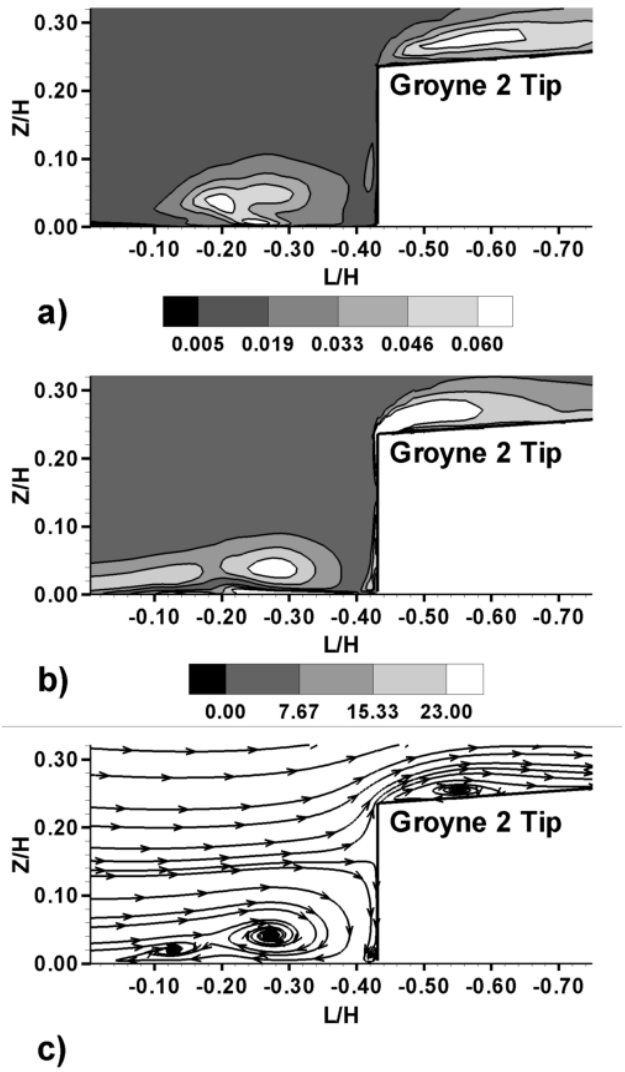

Figure 7. Visualization of the structure of the mean flow horseshoe vortex system around groyne 2 in a vertical section cutting through the groyne. The position of the section is shown in Figure 6. a) Nondimensional TKE, b) Nondimensional total vorticity magnitude, and c) 2D streamlines.

The elongated patches of high TKE and vorticity magnitude present over the top groyne face are due to the orientation of the groynes, which is against the flow in the present configuration. Thus, rather than forming a horizontal mixing layer at the lateral interface between the embayments and main channel, the mean flow is oriented at a high angle with the outer bank. Therefore, as the flow is convected past the extremity of the groyne, it separates. The quasi-steady separation bubble is seen in Figure 7c, although the high value of the Q isosurface in Figure 6 was not able to capture this eddy. Most of the TKE and vorticity amplification occurs within the separated part of the shear layer forming in the vicinity of the top groyne face.

Figure 8 shows distributions of non-dimensional mean friction velocity magnitude (u_*/u) and pressure root-mean-square (rms) fluctuations at the channel bottom surface. The black contour line in Figure 8 (top) corresponds to the critical sediment entrainment value (u_*/u = 0.064)

determined from the sediment size used in the loose bed experiments. However, sediment entrainment can occur outside of the region where $u_*/u > 0.064$ if pressure fluctuations are sufficiently high. This is why analysis of the pressure rms distribution (Figure 8 (bottom)) is required together with that of bed friction velocity.

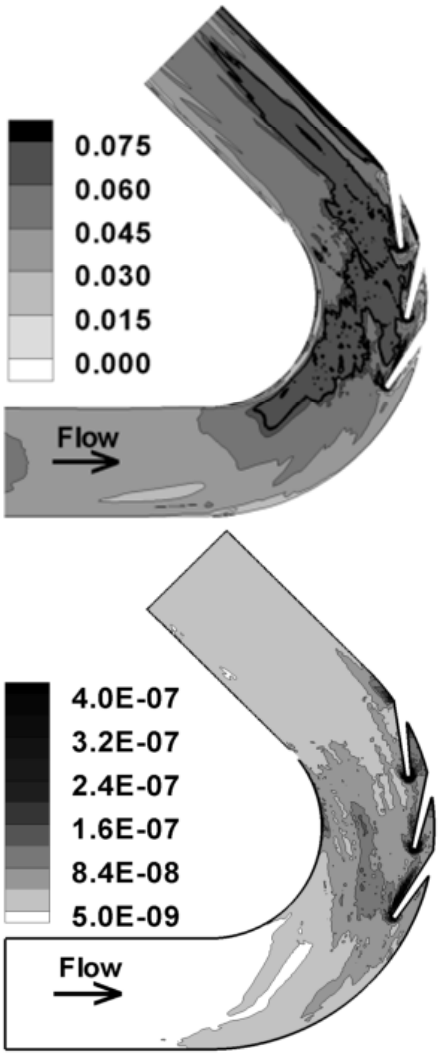

Figure 8. Distribution of nondimensional mean-flow friction velocity magnitude, u^*/u, (top) and pressure rms fluctuations, $<p'^2>/(\rho^2 U^4)$, (bottom). The black line corresponds to the critical friction velocity based on Shields` diagram.

Comparison of Figures 4a (Z/H = 0.25) and 8 shows that the correlation between the streamwise velocity distribution in the lower part of the channel, below the embayment top interface, and the bed friction velocity is quite high. This means that the streamwise velocity component provides the largest contribution to the bed friction velocity. The region of high values of u_*/u does not penetrate to the outer bank, though some relatively large values of u_*/u are observed near the downstream groyne faces, starting at their tip, over more than half of their length. This is due to the orientation of the groynes, that make a relatively small angle with the local mean flow direction. Consequently, a stronger separated shear layer develops on the downstream groyne side (Figure 6). This separated shear layer contains eddies that are advected within it. Some "shading" effect is observed for groyne 3. The intensity of pressure fluctuations is substantially smaller beneath the separated shear layer forming on the downstream side of groyne 3. The passage of these eddies explains the high values of pressure rms fluctuations in the bed regions beneath these shear layers. This is in contrast to when the groyne angle is 90^0 or larger, in which case the separated shear layers form a horizontal mixing layer between the groyne field and the main channel (e.g., see discussion in Constantinescu et al., 2009). Amplification of bed friction velocity close to the outer wall past the third groyne is in part related to a strong junction vortex in that region (see 135^0 section, Figure 4b).

As the region of high u_*/u values remains mostly situated outside of the inner part of the embayments, it proves that the present groyne configuration is an efficient way to protect against scour even when the groynes become submerged. However, regions of severe scour will occur within the channel. The very high values of bed friction velocity and pressure rms fluctuations suggest that the most severe scour will occur close to the extremity of the three groynes, particularly at the groyne tip. The loose bed experiments confirmed this, and the maximum scour depth was similar to that observed in the experiments without groynes. For the present case, it was expected that maximum scour would occur around the extremity of the groynes because they pointed in to and obstructed the flow (the groyne angle was only 25º, thus the local main channel flow made a small angle with each groyne). In fact, flow entered the embayment through most of the lateral face of each embayment and was eventually pushed out of the embayment close to the junction between the downstream groyne and outer bank.

Besides the presence of a strong horseshoe vortex system, the strong downflow parallel to the extremity face of each groyne is the main reason for the very large amplification of pressure rms fluctuations close to the groyne tips. Outside the embayments, regions of high pressure rms fluctuations do not exactly coincide with those of high bed friction velocity. Therefore relying only on bed friction velocity distribution is insufficient to characterize sediment entrainment capacity in a complex flow. Compared to bed friction velocity, pressure rms fluctuations are damped faster downstream of the third groyne. This is because the bed friction velocity is induced by the core of large streamwise velocities in the mean flow, while the pressure fluctuations are associated mostly with

the passage of large scale energetic eddies in a certain region.

5 CONCLUSIONS

This study revealed the complex interactions occurring between submerged groynes and the main channel flow developing within a channel bend during initial scour stages. Linkages were demonstrated between large-scale vortices and flow features near the bed and the bed friction velocity distribution. The main conclusions are given below.

1. The highest values of friction velocity and pressure fluctuations likely to induce scour occurred close to the groyne tips. These values were induced by the horseshoe vortices and the strong downflow. Friction velocities higher than the critical Shields value also occurred at the channel centerline near the groynes, along the inner bend near the bend entrance, and along the outer bank downstream of groyne 3.
2. Within the inner part of the embayments, friction velocities were low and recirculation was almost entirely absent, likely due to the orientation of the submerged groynes.
3. For this initial bed case the groynes were able to prevent high main channel velocities from reaching the outer bank in the area where the groynes were installed.
4. The LES revealed a complex set of vortices in the shear layer along the inner bend that may increase sediment erosion at the inner bend. If this erosion is of practical concern, one possible solution would be to install groynes at the inner bank. A comparison of the position and strength of these vortices when groynes are not present is needed to understand if groynes at the outer bank significantly increase the circulation and the erosion capability of the streamwise oriented vortices forming at the inner bank in bends of very sharp curvature.

The long-term goal of this study is to better understand how groynes interact with the main channel flow and to use this insight to propose new design criteria for the placement and spacing of groynes.

REFERENCES

Abad, J.D., Rhoads, B.L., Güneralp, I. and García, M.H. (2008). "Flow structure at different stages in a meander-bend with bendway weirs." J. Hydr. Engrg., 138(8), 1052-1063.

Constantinescu, S.G., Sukhodolov, A. and McCoy, A. (2009). "Mass exchange in a shallow channel flow with a series of groynes: LES study and comparison with laboratory and field experiments." Environ. Fluid Mech., Vol. 9(6), 587-615.

Devenport, W.J. and Simpson, R.L. (1990), "Time-dependent and time-averaged turbulence structure near the nose of a wing-body junction," J. Fluid Mech., Vol. 210, 23-55.

Kirkil, G. and Constantinescu, G. 2009. "Nature of flow and turbulence structure around an in-stream vertical plate in a shallow channel and the implications for sediment erosion." Water Resour. Res., 45, W06412.

Koken, M. and Constantinescu, G. (2008). "An investigation of the flow and scour mechanisms around isolated spur dikes in a shallow open channel: 1 Conditions corresponding to the initiation of the erosion and deposition process." Water Resour. Res., 44, W08406.

Koken, M. and Constantinescu, G. 2009. "An investigation of the dynamics of coherent structures in a turbulent channel flow with a vertical sidewall obstruction." Phys. Fluids, 21, 085104, DOI 10.1063/1.3207859.

Kuhnle, R.A., Jia, Y. and Alonso, C.V. (2008). "Measured and simulated flow near a submerged spur dike." J. Hydr. Engrg., 134(7), 916-924.

Mahesh, K., Constantinescu, S.G. and Moin, P. (2004). "A numerical method for large eddy simulation in complex geometries." J Comput..Phys., Vol. 197, 215-240.

Matsurra, T. (2004). "Stream-bank protection in narrow channel bends using 'barbs' – a laboratory study." M.A.Sc. Thesis, University of Ottawa, Ottawa, ON.

Minor, B., Rennie, C.D., and Townsend, R.D. (2007). "Barbs for river bend bank protection: application of a three-dimensional numerical model." Can. J. Civ. Eng., 34, 1087-1095.

McCoy, A., Constantinescu, G. and Weber, L. (2007). "A numerical investigation of coherent structures and mass exchange processes in channel flow with two lateral submerged groynes." Water Resour. Res., 43, W05445.

McCoy, A., Constantinescu, G. and Weber, L. (2008). "Numerical investigation of flow hydrodynamics in a channel with a series of groynes." J. Hydr. Engrg, 134(2), 157-172.

USDA. (2005). "Technical Note 23: Design of stream barbs." U.S. Department of Agriculture, Natural Resources Conservation Service, Portland, Oregon.

US Department of Transportation. (1985). "Design of spur-type streambank stabilization structures." Report No. FHWA/RD-84/101. National Technical Information Service, Springfield, Virginia, 98p.

Waterway Simulation Technology (WST) Inc. (2002). "Physical model test for bendway weir design criteria." Report ERDC/CHL TR-02-28, US Army Corps of Engineers.

Yossef, M.F.M. (2005). "Morphodynamics of rivers with groynes." M.Sc. Thesis, Delft University of Technology, Netherlands.

Zeng, J., Constantinescu, G., Blanckaert, K. and Weber, L. (2008). "Flow and bathymetry in sharp open-channel bends: Experiments and predictions." Water Resour. Res., 44, W09401.